# Anharmonic properties of the vibrational quantum computer

Meiyu Zhao and Dmitri Babikov[a)]
*Chemistry Department, Wehr Chemistry Building, Marquette University, Milwaukee, Wisconsin 53201-1881*

(Received 29 January 2007; accepted 10 April 2007; published online 24 May 2007)

We developed an efficient approach to study the coherent control of vibrational state-to-state transitions. The approximations employed in our model are valid in the regime of the low vibrational excitation specific to the vibrational quantum computer. Using this approach we explored how the vibrational properties of a two-qubit system affect the accuracy of subpicosecond quantum gates. The optimal control theory and numerical propagation of laser-driven vibrational wave packets were employed. The focus was on understanding the effect of the three anharmonicity parameters of the system. In the three-dimensional anharmonicity parameter space we identified several spots of high fidelity separated by low fidelity planar regions. The seemingly complicated picture is explained in terms of interferences between different state-to-state transitions. Very general analytic relationships between the anharmonicity parameters and the frequencies are derived to describe the observed features. Geometrically, these expressions represent planes in the three-dimensional anharmonicity parameter space. Results of this work should help to choose a suitable candidate molecule for the practical implementation of the vibrational two-qubit system.
 [DOI: 10.1063/1.2736693]

## I. INTRODUCTION

The idea to use vibrational states of a polyatomic molecule for universal quantum computation (QC) was first proposed by Tesch *et al.*[1] In this approach two vibrational eigenstates (typically, the ground and the first excited vibrational states) are used to represent $|0\rangle$ and $|1\rangle$ states of qubit. Different qubits are encoded into different normal vibration modes of a molecule and thus remain independent in the absence of external fields. All the quantum logics operations, starting with the simplest one-qubit flips and going to the more complicated multiqubit gates, can be applied to such a vibrational register using infrared laser pulses carefully prepared (shaped) in order to induce only the desired vibrational transitions while suppressing the interfering ones. Such an optimal pulse shape can be either predicted theoretically using the optimal control theory (OCT) (Ref. 2) or derived experimentally using the adaptive learning algorithms.[3–5]

Note that in this coherent control scheme the molecule remains in its ground electronic state and undergoes purely vibrational excitations. Consequently, the shaped laser pulses are required to cover the infrared part of the spectrum down to may be deep infrared. Since the existing pulse shaping techniques are only applicable to the visible light,[3–5] the experimental implementation of this vibrational QC principle is not yet possible but will undoubtedly become possible in the near future because the pulse shaping becomes more and more mature and steadily moves towards the infrared part of the spectrum.[6–9] Contrary to the experimental difficulties, the theoretical modeling of the vibrational quantum computer is relatively straightforward because the potential energy surface for the ground electronic state is usually well known and is typically not complicated. Furthermore, in the regime of the low vibrational excitation the vibrational structure of many molecules is accurately described simply by a set of normal mode vibration frequencies $(\omega_1, \omega_2, \ldots)$, *intramode* anharmonicities for every mode $(\Delta_1, \Delta_2, \ldots)$ and *intermode* anharmonicity parameters for each pair of modes $(\Delta_{12}, \ldots)$ These properties can be accurately predicted using the existing electronic structure theory methods. Alternatively, they can be borrowed from the spectroscopists. Due to these simplifications, the theoretical studies of the vibrational quantum computer are somewhat ahead of the experimental efforts in this field and it is clear that theory is playing an important guiding role.

Indeed, the vibrational QC is today a subject of active theoretical research and a number of theory papers have been published on this topic in the last few years. The pioneering series of papers by Vivie-Riedle and co-workers[1,10–12] has focused on the gas phase H–C≡C–H as a prototype molecule for a vibrational quantum computer. They showed that very short (700 fs) optimally shaped laser pulses are able to serve as quantum gates. This result demonstrated an important advantage of the vibrational quantum computer—its speed of gate operations, which is superior to all other known schemes proposed for QC. However, the reason for the choice of the $C_2H_2$ molecule was mainly historic: the authors of Refs. 1 and 10–12 performed some other coherent control studies of acetylene earlier and they had available the potential energy surface and the dipole moment function of this molecule.[13] An obvious drawback of $C_2H_2$ as a candidate for vibrational QC is that it has a very large frequency separation between the two IR-active vibrational modes (727 and 3289 $cm^{-1}$) used to encode the two qubits. This property makes it difficult to span and control both vibration modes

[a)]Author to whom correspondence should be addressed. Electronic mail: dmitri.babikov@mu.edu

 

simultaneously by the same single laser pulse, which is required in order to coherently implement the two-qubit gates.

In our first paper on the topic of vibrational QC (Ref. 14) we studied how the vibrational properties of the molecule affect the accuracy of one-qubit gates and the pulse duration required to perform accurate qubit transformations. We began with a diatomic OH molecule as a vibrational one-qubit system and have obtained optimal pulses for several one-qubit gates. This molecule possesses a large anharmonicity parameter $\Delta=90\ \mathrm{cm}^{-1}$ and has been used as a benchmark system in many coherent control studies. We then theoretically "tuned" the anharmonicity parameter through a broad range of $10\leqslant\Delta\leqslant110\ \mathrm{cm}^{-1}$, keeping the frequency $\omega=3964\ \mathrm{cm}^{-1}$ constant, and have optimized the pulse shape for each case. Using this model we showed that large anharmonicity parameter is a dominant factor in achieving the high fidelity of the quantum gates in the vibrational qubit. Thus, we demonstrated that when $\Delta$ is reduced to $30\ \mathrm{cm}^{-1}$ and below, the accuracy of 750 fs pulses drops rapidly. In the $\Delta>50\ \mathrm{cm}^{-1}$ region we observed a *high fidelity plateau* where the accuracy is 0.995 or better. We found that in such cases only a very few vibrational eigenstates are populated during the gate pulse, typically, just states $|0\rangle$, $|1\rangle$, and $|2\rangle$ with a negligible population of upper vibrational states. Finally, we demonstrated that the important effect of $\Delta$ is to help resolve and suppress the interfering transitions to the upper vibrationals states: $|2\rangle$, $|3\rangle$, $|4\rangle$, etc. We also showed that in those cases when the accuracy of gates is not very high (due to insufficient anharmonicity) some extra accuracy can be recovered by allowing a longer pulse duration. However, in order to achieve high fidelity subpicosecond gates in a practical implementation of the vibrational qubits, molecules with the values of at least 0.013 for the $\Delta/\omega$ ratio should be considered, i.e., $\Delta>50\ \mathrm{cm}^{-1}$ for $\omega=3964\ \mathrm{cm}^{-1}$ (for lower frequency modes a proportionally smaller anharmonicity should suffice). Later these conclusions were confirmed by Cheng and Brown.[15]

The search for a suitable molecule begun and several new candidates were considered, including $I_2$,[16] manganese pentacarbonyl bromide,[17] and even such an exotic vibrational system as $NH_3$ isolated inside the carbon nanotube.[18] Several other important properties of the vibrational qubits have been addressed in the recent literature. For example, controlling the relative phases of different state-to-state transitions proved to be important for the implementation of vibrational QC.[19–21] It was also proposed to combine several quantum gates, or even the entire quantum algorithm, within a single optimally shaped laser pulse.[16,20] New algorithms for the theoretical optimization of the pulse shape were proposed by Cheng and Brown.[15,22] Fundamental prospects of the vibrational state-to-state transitions, important in vibrational quantum computing, were studied by Sibert III and Gruebele and Weidinger and Gruebele.[23,24] A somewhat different scheme of using for QC the vibrational states of different *electronic* states was explored by Palao and Kosloff[25,26] and by Lidar and co-workers[27–29] and was first carried out experimentally by Vala *et al.*[30]

In this paper we continue our study of properties of the vibrational quantum computer using our approach of varying the amount of anharmonicity present in the system[14] but now we extend this model onto a two-qubit system. A nonlinear gas-phase molecule possesses $3N$-6 normal vibration modes but we focus on two suitable modes that form a decoherence-free subspace. These modes are chosen to represent two qubits (corresponding Hilbert space is shown schematically in Fig. 6 below). The ground vibrational state, overtones, and the combination state are used to represent $|00\rangle$, $|01\rangle$, $|10\rangle$, and $|11\rangle$ states of the two-qubit system, respectively. According to standard convention the first qubit is the *control* qubit and the second qubit is the *target* qubit. For example, the controlled NOT (CNOT) gate is represented as

$$|00\rangle \rightarrow |00\rangle, \tag{1a}$$

$$|01\rangle \rightarrow |01\rangle, \tag{1b}$$

$$|10\rangle \rightarrow |11\rangle, \tag{1c}$$

$$|11\rangle \rightarrow |10\rangle. \tag{1d}$$

This means that if the control qubit is in state $|0\rangle$ the state of the target qubit remains intact but, if the control qubit is in the state $|1\rangle$, the target qubit flips. The corresponding state-to-state transitions involve four vibrational states in the $2\times2$ space of the two-qubit system. Upper vibrational states can be populated during the gate pulse as well but by the end of the pulse action all the probability amplitude must be transferred to the appropriate final state of the two-qubit system.

The question we address now is this: How anharmonic must the two-qubit system be in order to reliably implement the two-qubit gates (such as CNOT) using subpicosecond optimally shaped laser pulses? It appears that the answer to this question is not straightforward, despite that we have a very similar question already answered for the case of the one-qubit system. At the time when we carried out our one-qubit study[14] we have also done some preliminary calculations on a two-qubit system. We hoped to obtain a reliable vibrational two-qubit system by simply taking two modes with large anharmonicities $\Delta_1$ and $\Delta_2$ (by analogy with the one-qubit case) but soon we recognized that having a significant intermode anharmonicity $\Delta_{12}$ is equally important for a two-qubit system. The two-qubit gates cannot be implemented on a system with $\Delta_{12}=0$ (this conclusion was also drawn recently in Ref. 31). Interestingly, taking all three anharmonicity parameters to be large ($\Delta_1$, $\Delta_2$, and $\Delta_{12}$ on the order of $100\ \mathrm{cm}^{-1}$) did not give us a good two-qubit system either, but at that time we could not explain why. The reason is now clear to us and the answer is given in this paper.

This paper is organized as follows: In Sec. II we construct and benchmark our two-qubit model and briefly review the pulse optimization procedure. Our results are presented and discussed in Sec. III. Conclusions are outlined in Sec. IV.

## II. THEORY

As usual, the evolution of the vibrational wave function satisfies the time-dependent Schrödinger equation,

$$i\frac{\partial}{\partial t}\psi(Q_1,Q_2,t)=\hat{H}\psi(Q_1,Q_2,t), \tag{2a}$$

$$\hat{H}=\hat{H}_0-\varepsilon(t)\cdot\mu(Q_1,Q_2), \tag{2b}$$

$$\hat{H}_0\equiv-\frac{1}{2m_1}\frac{\partial^2}{\partial Q_1^2}-\frac{1}{2m_2}\frac{\partial^2}{\partial Q_2^2}+V(Q_1,Q_2). \tag{2c}$$

Here $Q_1$ and $Q_2$ are the two normal mode coordinates, $\hat{H}_0$ is molecular Hamiltonian in the absence of external field, $\varepsilon(t)$ is the time-dependent electric field of the shaped laser pulse, and $\mu(Q_1,Q_2)$ is the dipole moment function of the molecule. In Ref. 14 we demonstrated that under the action of an optimized laser pulse on a vibrational qubit only very few vibrational eigenstates of $\hat{H}_0$ acquire a non-negligible population. In such a case it is most convenient to expand the wave function in a basis of the vibrational eigenstates,

$$\psi(Q_1,Q_2,t)=\sum_{ij}c_{ij}(t)|\varphi_{ij}(Q_1,Q_2)\rangle e^{-iE_{ij}t}, \tag{3}$$

where the energy eigenvalues and eigenfunctions of $\hat{H}_0$ are labeled by two quantum numbers $i$ and $j$ that represent the number of vibration quanta in each normal mode. In practice, it is enough to include only five states in each mode, 25 states in total in the sum of Eq. (3), so that $0\leqslant i\leqslant 4$ and $0\leqslant j\leqslant 4$. Substituting this expansion into the Schrodinger Equation [Eq. (2a)] and projecting the result onto the vibrational eigenstates $e^{+iE_{kl}t}\langle\varphi_{kl}(Q_1,Q_2)|$ we obtain the following system of coupled equations for the probability amplitudes:

$$\dot{c}_{ij}(t)=i\varepsilon(t)\sum_{kl}c_{kl}(t)M_{kl,ij}e^{-i(E_{ij}-E_{kl})t}, \tag{4}$$

where we introduced the standard dipole moment matrix **M**. The analysis of these equations is straightforward: The time evolution of the probability amplitudes is driven by the magnitude of the electric field, by the values of corresponding elements of the dipole moment matrix, and finally by the energy separation of corresponding vibrational states. In the absence of the field or of the dipole moment the probability amplitudes remain constant. Note that the time propagation of these equations requires only the knowledge of energy eigenvalues ($E_{ij}$) and of the elements of the dipole moment matrix ($M_{ij,kl}$) which are numbers. Vibrational eigenfunctions $\varphi_{ij}(Q_1,Q_2)$ are no longer present in the equations explicitly.

In an approximate treatment of Eqs. (4) one can use simplifying assumptions to compute the values of $E_{ij}$ and $M_{ij,kl}$. Thus, it is well known that for a variety of molecules the energy spectrum of lower vibrational eigenstates is described reasonably well by the Dunham expansion,

$$E_{ij}=\omega_1\left(i+\tfrac{1}{2}\right)-\Delta_1\left(i+\tfrac{1}{2}\right)^2+\omega_2\left(j+\tfrac{1}{2}\right)-\Delta_2\left(j+\tfrac{1}{2}\right)^2-\Delta_{12}\left(i+\tfrac{1}{2}\right)\left(j+\tfrac{1}{2}\right), \tag{5}$$

where $\omega_1$ and $\omega_2$ correspond to harmonic frequencies, $\Delta_1$ and $\Delta_2$ are intramode anharmonicity parameters, and $\Delta_{12}$ describes the intermode anharmonicity or the coupling effect. This formula is used routinely to fit experimental data by tuning the values of all five parameters to minimize the rms deviation.[32] It is also a standard practice to fit eigenvalues obtained by sophisticated theoretical methods (such as diagonalization, etc.) using this or similar expressions[33] in order to give a simplified picture of the spectrum. In this work we use Eq. (5) to describe the spectrum of the vibrational two-qubit system and we vary the values of all three anharmonicity parameters ($\Delta_1$, $\Delta_2$, and $\Delta_{12}$) in the range from 40 to 120 $cm^{-1}$ in order to study the effect of anharmonicity. The values of $\omega_1$ and $\omega_2$ are kept constant in this study.

While doing this work we had in mind a proposal by the Los Alamos group[34] to use (for the practical demonstration of the vibrational QC principle) the low temperature molecular crystals such as naphthalene, $C_{10}H_8$, at 4 K. In such conditions the interaction between different naphthalene molecules is relatively weak and the vibrational character of isolated molecules is preserved. Decoherence rates are controlled by cooling. We performed electronic structure calculations for $C_{10}H_8$ using B3LYP/6-31G** level of theory and GAUSSIAN03 suite of *ab initio* programs[35] to determine the normal vibration modes, frequencies, and corresponding effective masses. To represent the two-qubit system we selected two bright IR-active modes at $\omega_1=1615$ $cm^{-1}$ and $\omega_2=1423$ $cm^{-1}$. The reduced masses are $m_1=3.23$ a.u. and $m_2=2.89$ a.u. The choice in mid-infrared range was made for generality but several other choices are possible using the normal modes of $C_{10}H_8$ molecule.

Elements of the dipole moment matrix in Eq. (4) should be computed as

$$M_{kl,ij}\equiv\langle\varphi_{kl}(Q_1,Q_2)|\mu(Q_1,Q_2)|\varphi_{ij}(Q_1,Q_2)\rangle_{Q_1Q_2}, \tag{6}$$

where the indices $i$ and $j$ are used to label the initial states, while the indices $k$ and $l$ are used to label the final states. In general, the dipole moment $\mu$ is a function of two coordinates $Q_1$ and $Q_2$, but in the vicinity of the equilibrium point all quadratic and higher order terms in the Taylor series expansion can be neglected and the dipole moment function can be described simply by

$$\mu(Q_1,Q_2)\approx\mu_0+\mu_1Q_1+\mu_2Q_2. \tag{7}$$

Indeed, a closer inspection of the dipole moment surfaces of the molecule studies as candidates for quantum computation so far (see Refs. 1, 10, and 17, for example) shows that in the range of interest those surfaces are very close to planes. Finally, since we exploit the regime of low vibrational excitation we can approximate the two-dimensional vibrational eigenstates in Eq. (6) by a product of harmonic oscillator functions for the normal vibration modes,

$$|\varphi_{ij}(Q_1,Q_2)\rangle\approx|\varphi_i(Q_1)\varphi_j(Q_2)\rangle=|i,j\rangle. \tag{8}$$

We use this approximation only in the calculations of the dipole moment matrix elements in Eq. (6) and it is expected to work reasonably well for this purpose. The substitution of Eqs. (7) and (8) into Eq. (6) gives

$$M_{kl,ij} = \mu_0 \langle k|i\rangle_{Q_1} \langle l|j\rangle_{Q_2} + \mu_1 \langle k|Q_1|i\rangle_{Q_1} \langle l|j\rangle_{Q_2} + \mu_2 \langle k|i\rangle_{Q_1} \langle l|Q_2|j\rangle_{Q_2}$$
$$= \mu_0 \delta_{k,i}\delta_{l,j} + \frac{\mu_1}{\sqrt{2m_1\omega}}(\sqrt{k}\,\delta_{k,i+1} + \sqrt{k+1}\,\delta_{k,i-1})\delta_{l,j} + \frac{\mu_2}{\sqrt{2m_2\omega_2}}(\sqrt{l}\,\delta_{l,j+1} + \sqrt{l+1}\,\delta_{l,j-1})\delta_{k,i}, \quad (9)$$

where the properties of Hermit polynomials[36] were used. This expression leads to the well known selection rules for infrared transitions: $\Delta i = \pm 1$, $\Delta j = \pm 1$.[37] The values of parameters $\mu_0 = 0$ and $\mu_1 = \mu_2 = 0.4$ a.u. were used in this study.

Note that all the assumptions made here are justified by the fact that the vibrational excitation is low and the wave function is localized near the equilibrium position. Another way to look at our model is from the standpoint of the perturbation theory, where in the zero-order Hamiltonian, all the anharmonic terms in the potential energy function $V(Q_1, Q_2)$ of Eq. (2c) are neglected. This way the zero-order energies and wave functions are those of a two-dimensional harmonic oscillator. But such a system cannot be controlled and at least the first-order correction to energies is required, which is given in Eq. (5). It is usual in the perturbation theory to use the wave functions of lower order with (more accurate) energies of the higher order. Thus, we simply use zero-order wave functions and first-order energies. To access the accuracy of our model we present some benchmark calculations later in this section.

In order to theoretically design a shape for the pulse, which can serve as a quantum gate, the monotonically convergent numerical algorithm[2] derived from the OCT is usually employed. In its traditional implementation this algorithm is used to optimize the pulse shape $\varepsilon(t)$ for a transfer of the entire population from a given initial vibrational state $\varphi_{ij}$ to a chosen final state $\varphi_{kl}$ within a specified time interval $T$. This is achieved by maximizing a relatively simple objective functional.[2,38,39] For quantum computation, however, the laser pulse should carry out a unitary transformation of the vibrational qubit states. For example, for the gate CNOT we have to find a pulse which induces not just one but four transitions between the states of the two-qubit system simultaneously, as required by Eqs. (1a)–(1d). Thus, if the system was initially in the vibrational state $|10\rangle$ it should be driven into the state $|11\rangle$, but if it was initially in the state $|11\rangle$ it should be driven into the state $|10\rangle$, etc., according to Eqs. (1a)–(1d). One universal pulse $\varepsilon(t)$ should be able to perform each of the four transformations in Eqs. (1a)–(1d). Which one is actually performed depends only on the initial state of the two-qubit system. Therefore, it is necessary to optimize the population transfer for four transitions simultaneously. Such a problem can be addressed by maximizing the functional where the sum over the four transitions is introduced,[2,10–18]

$$K \equiv -\int_0^T \alpha|\varepsilon(t)|^2 dt + \sum_{i,j=0}^{1} |\langle \psi_{ij}(T)|\varphi_{kl}\rangle|^2 - \sum_{i,j=0}^{1} 2\,\mathrm{Re}\left\{\langle \psi_{ij}(T)|\varphi_{kl}\rangle \int_0^T \langle \psi_{ij}(t)|i\hat{H} + \frac{\partial}{\partial t}|\psi_{ij}(t)\rangle dt\right\}. \quad (10)$$

Here the $\psi_{ij}(t)$'s are laser-driven time-dependent wave functions for each case (subscript specifies the initial state). Each term $|\langle \psi_{ij}(T)|\varphi_{kl}\rangle|^2$ represents an overlap of the final wave function with the corresponding target state and these are maximized. The sum is over the four state-to-state transitions of interest; for the gate CNOT we should include $\varphi_{00} \rightarrow \varphi_{00}$, $\varphi_{01} \rightarrow \varphi_{01}$ and $\varphi_{10} \rightarrow \varphi_{11}$ and $\varphi_{11} \rightarrow \varphi_{10}$ transitions according to Eqs. (1). The first term in Eq. (10) is required to minimize the energy of the pulse and also to constrain its smooth switching of on and off. The last term ensures that the evolution of the wave functions $\psi_{ij}(t)$ satisfies the time-dependent Schrödinger equation. The maximization of this functional leads to a set of four time-dependent Schrödinger equations to be propagated forward and backward in time using $\varphi_{ij}$'s and corresponding $\varphi_{kl}$'s, respectively, as boundary conditions. The optimal field $\varepsilon(t)$ is then determined iteratively.[2]

The accuracy of the qubit transformation performed by the laser pulse or gate *fidelity* is assessed by computing the average of transition probabilities over the four transitions,

$$F = \langle P \rangle = \frac{1}{4}\sum_{i,j=0}^{1} |\langle \varphi_{kl}|\psi_{ij}(T)\rangle|^2. \quad (11)$$

As optimization proceeds, we monitor the value of $F$ obtained after each iteration step and we stop iterations when the fidelity cannot be further improved. If the probability transfer achieved by the pulse is accurate for each optimized transition ($F \approx 1$), the relative phases of different transitions in Eqs. (1a)–(1d) can be "adjusted" after the pulse, employing the recently proposed approach of free evolution.[21] Using this method one should be aware that such a time delay between the gate pulses will increase the overall time required for the execution of a quantum algorithm.[21] Other methods to control phases are known[19,20,25,26] but we found that employing those leads to a slower convergence.

In order to test the accuracy of the model developed here we decided to reproduce the results of Ref. 14, where the exact energies, eigenfunctions, and an accurate dipole moment function of the OH molecule were used in the time propagation and pulse optimization. Note that here we use only a limited amount of information about the molecule, namely, the values of $\Delta = 90\ \mathrm{cm}^{-1}$, $\omega = 3978\ \mathrm{cm}^{-1}$, $\mu_0 = -0.30$ a.u., and $\mu_1 = 0.27$ a.u. obtained for the stationary point of OH. Using this data as input to our model we performed an optimization of the 750 fs pulse for the gate NOT, as in Ref. 14. The pulse shape obtained was basically indistinguishable from that of Ref. 14 and the time evolution of populations of the qubit states during the gate pulse was practically identical to that of Ref. 14 (see Fig. 2 in Ref. 14). The remarkable success of the simple model is due to the

low vibrational excitation regime. Note that the OH molecule is not a simple case and these benchmark calculations represent a really tough test of approximations used in our model because the OH molecule is very anharmonic. This case is also very important since the value of $\Delta=90$ cm$^{-1}$ belongs to the high fidelity plateau and allows us to obtain very accurate subpicosecond quantum gates.

## III. RESULTS AND DISCUSSION

As explained in the previous section, we vary the values of $\Delta_1$, $\Delta_2$, and $\Delta_{12}$ in the range from 40 to 120 cm$^{-1}$ using 10 cm$^{-1}$ step sizes, perform the pulse optimization for CNOT gate, and compute the pulse fidelity $F$ for each considered case. Overall, we performed optimizations on a $9\times9\times9$ three-dimensional grid in the $(\Delta_1,\Delta_2,\Delta_{12})$ space, for 729 sets of parameters in total, and constructed an accurate three-dimensional (3D)-spline interpolation of $F$ between the calculated points. Thus, the fidelity $F$ can be thought as a continuous function of three independent variables: $\Delta_1$, $\Delta_2$, and $\Delta_{12}$. Two views of the entire "data cube" are shown in Fig. 1 as $F(\Delta_1,\Delta_2,\Delta_{12})$. The color palette is used to show the value of $F$ in the range from 0.5 (violet) to 1.0 (red), with $F\sim0.8$ shown in green and $F\sim0.9$ in yellow. The overall picture is rather complicated. Briefly, we have identified *two main regions of high fidelity* in the $(\Delta_1,\Delta_2,\Delta_{12})$ space: A larger A region with a fidelity in the range of $0.97<F<0.9997$, and a smaller B region where the fidelity is somewhat lower, $0.90<F<0.985$. These two regions are separated by a plane in 3D-space referenced hereafter as the A/B plane, in the vicinity of which the fidelity drops significantly, to roughly $F\sim0.85$. We also observed another planar region in the $(\Delta_1,\Delta_2,\Delta_{12})$ space where the fidelity is exceptionally low, in the range of $0.5<F<0.6$. Finally, we found the third plane which breaks the A region onto two sub regions: $A_1$ and $A_2$. In the vicinity of this $A_1/A_2$ plane the fidelity is also reduced (slightly) to at least $F\sim0.985$. Some of these features are reflected on the surface of the data cube and can be seen in Fig. 1. A detailed analysis of these features is presented further in this section.

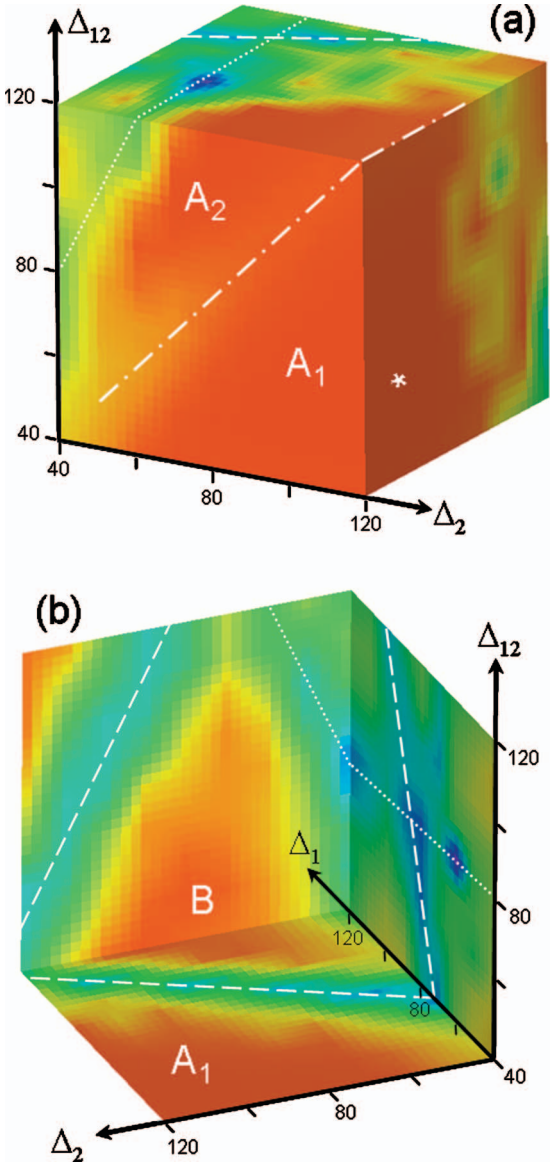


FIG. 1. (Color) Fidelity of the 750 fs gate CNOT in a model study as a function of three anharmonicity parameters of the system: $\Delta_1$, $\Delta_2$, and $\Delta_{12}$. Red color indicates fidelity close to one. The three high fidelity regions are labeled as $A_1$, $A_2$, and B. The point of highest fidelity is indicated by a star. The three low fidelity planes are indicated by dotted, dashed, and dot-dashed lines. Two complementary views of the data cube are given as (a) and (b).

### A. A region, highest fidelity

This high fidelity region of $(\Delta_1,\Delta_2,\Delta_{12})$ space is clearly seen in Fig. 1 and is characterized by large values of $\Delta_2$ and small values of $\Delta_1$. It is located roughly in the range of $\Delta_2>80$ cm$^{-1}$ and $\Delta_1<80$ cm$^{-1}$, extends through the entire range of $\Delta_{12}$, and occupies about 20% of the entire volume of the data cube. The maximum value of fidelity $F_{\max}=0.9997$ is found at the point $(\Delta_1,\Delta_2,\Delta_{12})=(55,120,65$ cm$^{-1})$ which is indicated in Fig. 1(a) by a star. In a broad vicinity of this point, $\pm15$ cm$^{-1}$ in any direction, the fidelity remains very high as well, exceeding the value of $F=0.999$. For the points in this range the optimal pulse shape is especially simple. A typical example is given in Fig. 2(a) for the point $(\Delta_1,\Delta_2,\Delta_{12})=(50,110,40$ cm$^{-1})$. The optimized pulse consists of two sub pulses. The first subpulse creates an intermediate superposition of the vibrational states in the middle of the pulse duration interval and the second subpulse completes the necessary transformation of the qubit state. The time evolution of populations of the qubit states is shown in Figs. 2(b)–2(e) for the four transitions in Eq. (1) optimized simultaneously for this gate. The population transfer is basically direct from the initial state to the final state with only a negligible population of upper vibrational states. These results are consistent with data presented in Refs. 17 and 31.

The fact that the highest value of the fidelity $F_{\max}$ is achieved at the point characterized by the maximum value of $\Delta_2=120$ cm$^{-1}$ is not surprising since the second qubit is used here as the target qubit and the conclusions of our one-qubit study[14] should be applicable to this qubit. In order to understand the composite effect of $\Delta_1$ and $\Delta_{12}$ we use the transition frequency diagram shown in Fig. 3, where a set of vertical lines represents state-to-state transition frequencies in the spectrum of the system. It is enough to include only the frequencies for transitions between the four lower vibrational

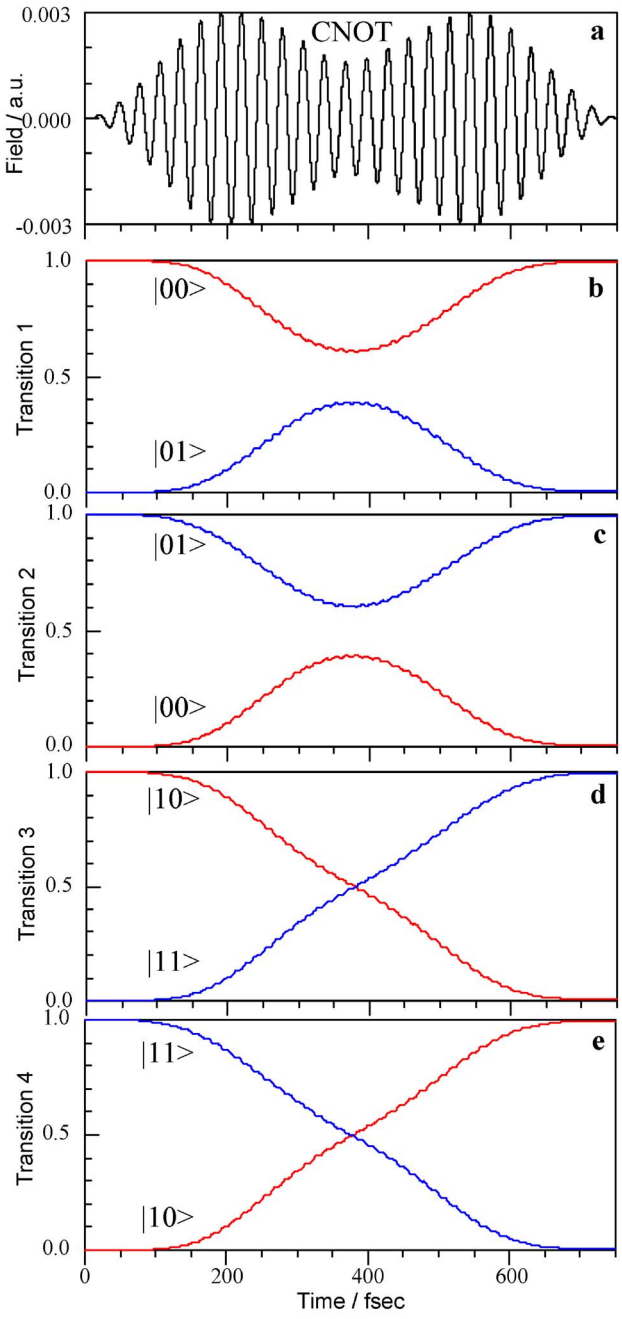


FIG. 2. (Color online) Conditional NOT in a typical two-qubit system. (a) Optimally shaped 750 fs laser pulse; [(b)–(e)] population transfer between the qubit states during the pulse for state-to-state transitions given by Eqs. (1a)–(1d).

states in each mode. Subject to the selection rules $\Delta i = \pm 1$ and $\Delta j = \pm 1$, this includes 12 transition frequencies for each mode or 24 frequencies in total. The solid lines in Fig. 3 are used for the second (target) mode while the dashed lines are used for the first (control) mode. To simplify the analysis the frequencies characterized by equal values of $i$ and $k$ (or equal values of $j$ and $l$) are connected into a group by a horizontal line. For example, the group of the lines located furthest to the right in Fig. 3 corresponds to the frequencies of $|0j\rangle \rightarrow |1j\rangle$ transitions with $j=\{0,1,2,3\}$. The group of lines located furthest to the left Fig. 3 corresponds to the frequencies of $|i2\rangle \rightarrow |i3\rangle$ transitions with $i=\{0,1,2,3\}$, and so on. The

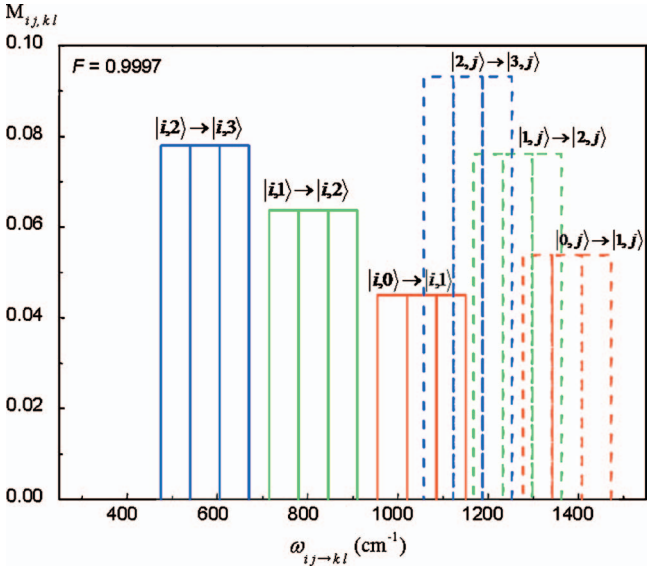


FIG. 3. (Color) Transition frequency diagram for a model system represented by the highest fidelity point $(\Delta_1,\Delta_2,\Delta_{12})=(55,120,65\ \mathrm{cm}^{-1})$. Twenty four frequencies are shown, none are in resonance. See text for details.

vertical axis in Fig. 3 is used to show the values of the corresponding dipole moment matrix elements.

One property of the spectrum presented in Fig. 3 is a large separation of frequencies for transitions in the second mode, including the transitions between the states of the target qubit. This behavior is controlled mostly by $\Delta_2$ but also by $\Delta_{12}$ and is seen as a large separation of different groups of solid lines. The second important property is the sparseness of the spectrum in the region where the different groups of transitions overlap. Namely, the 14 transition frequencies in the range of 1000–1400 $\mathrm{cm}^{-1}$ in Fig. 3 are almost equidistant with the step of roughly 30 $\mathrm{cm}^{-1}$, i.e., are maximally detuned. This behavior is affected by both $\Delta_1$ and $\Delta_{12}$.

### B. Plane of lowest fidelity

Inside of the data cube shown in Fig. 1 there is a region with exceptionally low fidelity of the pulses, roughly $F_{\min} \sim 0.5$. Several examples include the points characterized by $(\Delta_1,\Delta_2,\Delta_{12})=(60,40,80\ \mathrm{cm}^{-1})$, $(100,50,100\ \mathrm{cm}^{-1})$, and $(70,60,120\ \mathrm{cm}^{-1})$. These cases are practically useless but it is methodologically important to understand what makes these sets of anharmonicity parameters so unsuitable for the representation of the vibrational qubit states. Indeed, this result means that a large value of $\Delta_{12}=80\ \mathrm{cm}^{-1}$, $100\ \mathrm{cm}^{-1}$, or even $120\ \mathrm{cm}^{-1}$ is, by itself, not sufficient to guarantee the controllability of the system.

In order to exhibit this region of low fidelity points we used a tool which allows us to see only the data within a given range of values, making the rest of the data transparent. In Fig. 4(a) we used the window of $F<0.6$. A number of low fidelity points can be seen here very clearly. They are located in the region which is characterized by small $\Delta_2$ and large $\Delta_{12}$ and extends through the entire range of $\Delta_1$. This last property means that the vibrational transitions along the first (control) mode must be unimportant for the understanding of this effect and we can focus on the analysis of transi-

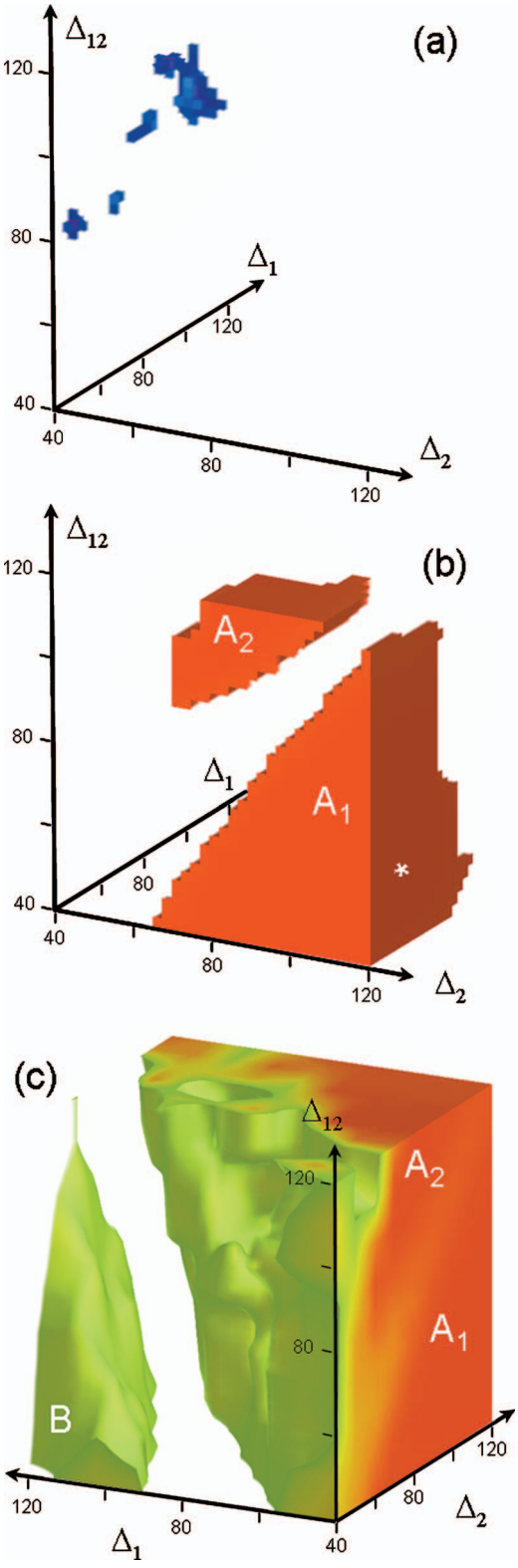


FIG. 4. (Color) Three-dimensional views of the main features of the data cube shown in Fig. 1: (a) the lowest fidelity region, (b) the gap between the regions $A_1$ and $A_2$, and (c) the gap between regions A and B. See text for details.

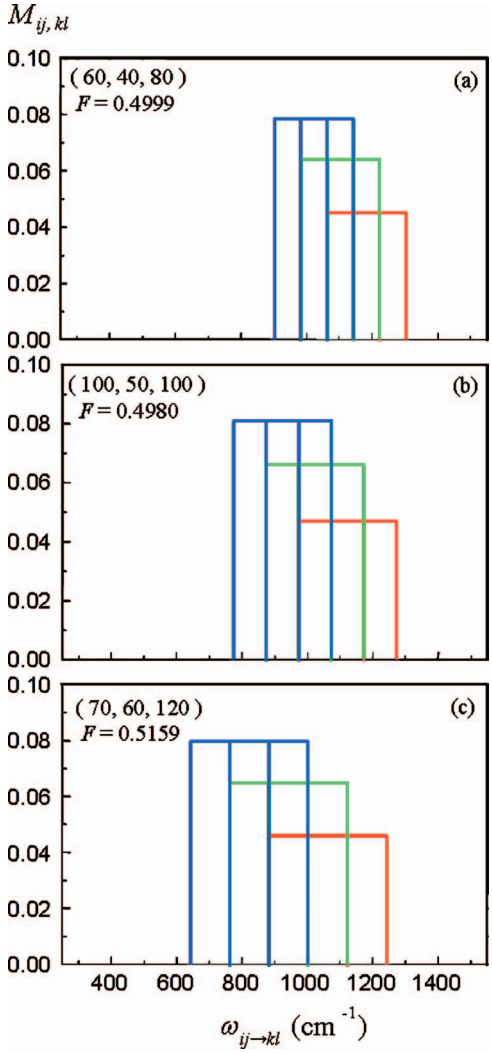


FIG. 5. (Color) Transition frequency diagrams for three typical points from the lowest fidelity plane. Twelve frequencies of the target mode are shown. Multiple resonances are clearly seen.

tions along the second (target) mode. These are presented in Figs. 5(a)–5(c) for the three sets of $(\Delta_1, \Delta_2, \Delta_{12})$ discussed in the previous paragraph. A striking feature of these systems becomes immediately obvious: The frequencies of $|i,j\rangle \to |i,j+1\rangle$ transitions for $j \geqslant 1$ coincide with the frequencies of $|i+1,j-1\rangle \to |i+1,j\rangle$ transitions. Note that for $j \geqslant 2$ they also coincide with the frequencies of $|i+2,j-2\rangle \to |i+2,j-1\rangle$ transitions, and so on. In Fig. 6(a) the sets of equivalent arrows are used to indicate different state-to-state transitions that are in resonance with each other in this case. We see that one of the transitions in the target qubit, $|10\rangle \to |11\rangle$, is in resonance with $|01\rangle \to |02\rangle$ transition, which further connects it to a ladder of transitions to all upper states. It is clear that in such a system transitions between the qubit states cannot be isolated from the interfering transitions and cannot be controlled selectively.

Finally, using Eq. (5) to express frequencies for the resonant transitions, such as $|i,j\rangle \to |i,j+1\rangle$ and $|i+1,j-1\rangle \to |i+1,j\rangle$, equating those expressions, and cancelling equal terms we came up with a very simple analytic relationship,

$$\Delta_{12} = 2\Delta_2. \tag{12}$$

Note that here both harmonic frequencies $\omega_1$ and $\omega_2$ cancel, as well as the anharmonicity of the control qubit $\Delta_1$. Coordinates of the three typical points from the $F_{\min} \sim 0.5$ region, discussed in the first paragraph of this section and analyzed in Figs. 5(a)–5(c), satisfy this equation. In general, this for-

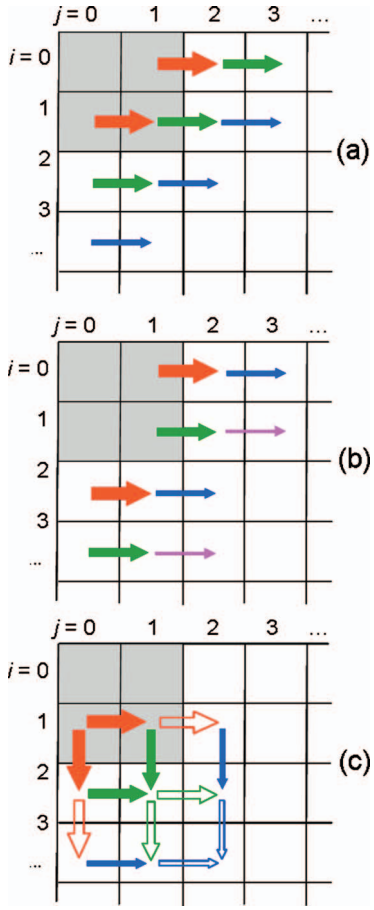


FIG. 6. (Color) Typical interference patterns for the three low fidelity planes: (a) the lowest fidelity plane, (b) the $A_1/A_2$ plane, and (c) the A/B plane. Resonant transitions are shown by equivalent errors.

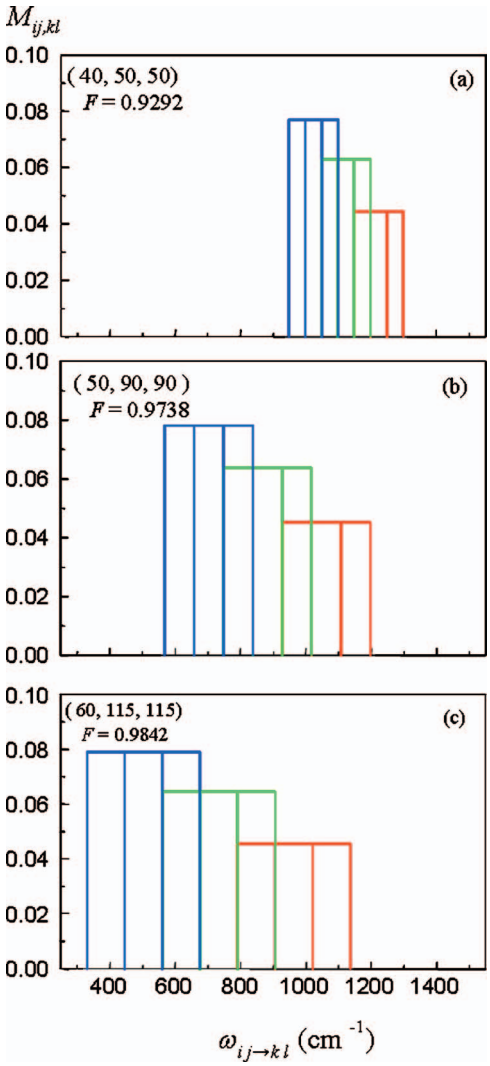


FIG. 7. (Color) Transition frequency diagrams for three typical points from the $A_1/A_2$ plane. Twelve frequencies of the target mode are shown. Multiple resonances are clearly seen. Compare to the frequency diagrams of Fig. 5.

mula defines a plane in $(\Delta_1,\Delta_2,\Delta_{12})$ space. Such a plane is parallel to the $\Delta_1$ axis and is perpendicular to the $(\Delta_2,\Delta_{12})$ plane. All the lowest fidelity points in the $F_{\min}\sim 0.5$ region either belong to this plane or are found very close to it, which is clearly seen in Fig. 4(a). Further analysis shows that in the vicinity of this plane, $\pm 5$ cm$^{-1}$, the fidelity $F$ slightly increases but still remains very poor in the range of $F_{\min}\sim 0.60-0.65$. Clearly, the lowest fidelity plane (12) and its vicinity should be avoided when choosing a candidate molecule for quantum computation.

### C. $A_1/A_2$ plane

The other prominent feature of the data cube is a plane in the middle of the high fidelity A region where the value of $F$ drops abruptly to $F\sim 0.985$ and below. This feature is illustrated in Fig. 4(b) using data cropping with an $F>0.987$ window. It is seen very clearly that this region of lower fidelity is roughly planar, occupies the space near the diagonal line of the $(\Delta_2,\Delta_{12})$ plane, and extends through the entire range of $\Delta_1$. Three typical points from this area are $(\Delta_1,\Delta_2,\Delta_{12})=(40,50,50\ \text{cm}^{-1})$, $(50,90,90\ \text{cm}^{-1})$, and $(60,115,115\ \text{cm}^{-1})$. The last point is especially surprising, because at this point both important anharmonicity parameters become very large, $\Delta_2$ and $\Delta_{12}=115$ cm$^{-1}$, but the fidelity remains relatively low, $F=0.984$. The transition frequency diagrams for these three points are given in Fig. 7 and even a quick look at these pictures reveals a number of resonant frequencies. Namely, the frequencies of $|i,j\rangle\to|i,j+1\rangle$ transitions for $j\geqslant 1$ coincide with the frequencies of $|i+2,j-1\rangle\to|i+2,j\rangle$ transitions. A scheme is given in Fig. 6(b) in order to explain this effect. Although this scheme is somewhat similar to that shown in Fig. 6(a), there are two important differences. First of all, none of the transitions between the qubit states is now in resonance with any other transition. This allows for better control of the state-to-state transitions in the qubit. Second, the interfering transitions, such as $|20\rangle\to|21\rangle$ and $|01\rangle\to|02\rangle$, are further away from each other (by one more quantum of $i$) compared to the case shown in Fig. 6(a). Due to these two properties, the interference (although still occurs) is less efficient compared to the case shown in Fig. 6(a) and the fidelity of qubit transformations is not that poor.

As before, we can use Eq. (5) to express frequencies for the resonant transitions $|i,j\rangle\to|i,j+1\rangle$ and $|i+2,j-1\rangle\to|i+2,j\rangle$. Equating these frequencies allowed us to cancel $\omega_1$, $\omega_2$, and $\Delta_1$. The resultant equation is simply

$$\Delta_{12} = \Delta_2. \tag{13}$$

This formula also defines a plane in the three-dimensional $(\Delta_1, \Delta_2, \Delta_{12})$ space and again it is parallel to the $\Delta_1$ axis and is perpendicular to the $(\Delta_2, \Delta_{12})$ plane. This $A_1/A_2$ plane is clearly seen in Fig. 4(b). Although the fidelity drop here is not as dramatic as in the lowest fidelity plane, this is a very "dangerous" region of the three-dimensional $(\Delta_1, \Delta_2, \Delta_{12})$ space because it extends into the range of large $\Delta_2$, which is attractive for the realization of the vibrational qubit. Thus, one should be very careful there and try to avoid the $A_1/A_2$ plane.

Comparing Fig. 4(a) to Fig. 4(b) or the diagram in Fig. 5 to that of Fig. 7, we see that the two low fidelity planes discussed above exhibit a number of similar features. For example, the first of them describes situations when the $|01\rangle \rightarrow |02\rangle$ transition interferes with the $|10\rangle \rightarrow |11\rangle$ transition, while the second describes situations when the same $|01\rangle \rightarrow |02\rangle$ transition interferes with $|20\rangle \rightarrow |21\rangle$ transition [compare Fig. 6(a) to Fig. 6(b)]. Thus, the $|01\rangle \rightarrow |02\rangle$ transition plays a special role here and will be referenced hereafter as the *key* transition. One can ask, are there other similar situations when the key transition interferes with some other transition and causes appearance of a low fidelity plane analogous to those discussed above? Two possibilities of this kind can be imagined, one where the key transition interferes with $|30\rangle \rightarrow |31\rangle$ transition, and another where the key transition interferes with $|00\rangle \rightarrow |01\rangle$ transition. The last possibility represents the worst case scenario because the $|00\rangle \rightarrow |01\rangle$ transition is a transition between two states of the target qubit and also because one of these states, $|01\rangle$, is linked by the key transition to the upper vibrational states. A transition frequency diagram for this case would show that the three groups of frequencies completely coincide. An equation for such a plane can be derived as well and is simply $\Delta_{12}=0$. This trivial case was discussed in the Introduction and describes uncontrollable systems. Note that the $\Delta_{12}=0$ plane is outside of our data cube.

The second possibility leads to the equation $\Delta_{12}=\frac{2}{3}\Delta_2$. We carefully inspected this region of the $(\Delta_1, \Delta_2, \Delta_{12})$ space in our data cube but we could not find any abrupt drop of fidelity there. This certainly means that the $|30\rangle \rightarrow |31\rangle$ transition is too far away from the key transition and, even if they are in resonance the population leakage from the qubit states, is not efficient anymore. Furthermore, this region of the $(\Delta_1, \Delta_2, \Delta_{12})$ space is characterized by a gradual reduction of the fidelity (due to $A_1/A_2$ plane) so that this larger effect may simply hide the smaller effect due to the resonance between the key transition and $|30\rangle \rightarrow |31\rangle$. Thus, we conclude that the two low fidelity planes given by Eqs. (12) and (13) are the only two existing regions of low fidelity of this kind.

### D. A/B plane

We finally focus on a plane which separates the B region from the A region. The B region is located in the range of large values of $\Delta_1$, medium $\Delta_2$, and small $\Delta_{12}$ as seen in Fig. 1. The fidelity here is not as high as in the A region but it still reaches the value of $F \sim 0.985$. The presence of the A/B plane is evident from Fig. 4(c) where we used data cropping and a window of $F > 0.85$. This view exhibits a planar region, 10–20 $cm^{-1}$ thick, where the fidelity drops below $F = 0.85$. Note that this plane is not parallel to any axis and passes through the entire data cube. In many points in the close vicinity of the A/B plane the fidelity drops to about $F \sim 0.7$. Several typical points from this region are $(\Delta_1, \Delta_2, \Delta_{12}) = (120, 120, 45\ cm^{-1})$, $(105, 80, 65\ cm^{-1})$, and $(100, 45, 115\ cm^{-1})$. The transition frequency diagrams for these cases are given in Fig. 8. A feature common to all these systems is a resonance between the $|i,j\rangle \rightarrow |i,j+1\rangle$ transition frequencies for $i \geqslant 1$, $j=0$ and the $|j+1, i-1\rangle \rightarrow |j+2, i-1\rangle$ transition frequencies. Note that indices are interchanged here, which means that the transitions along the second (target) mode are in resonance with corresponding transitions along the first (control) mode. In this region of the $(\Delta_1, \Delta_2, \Delta_{12})$ space we also found many points where in addition to such $j=0$ transitions some of the $j=1$ transitions, characterized by the same relationships, are in resonance with each other as well. The schematic representation of this

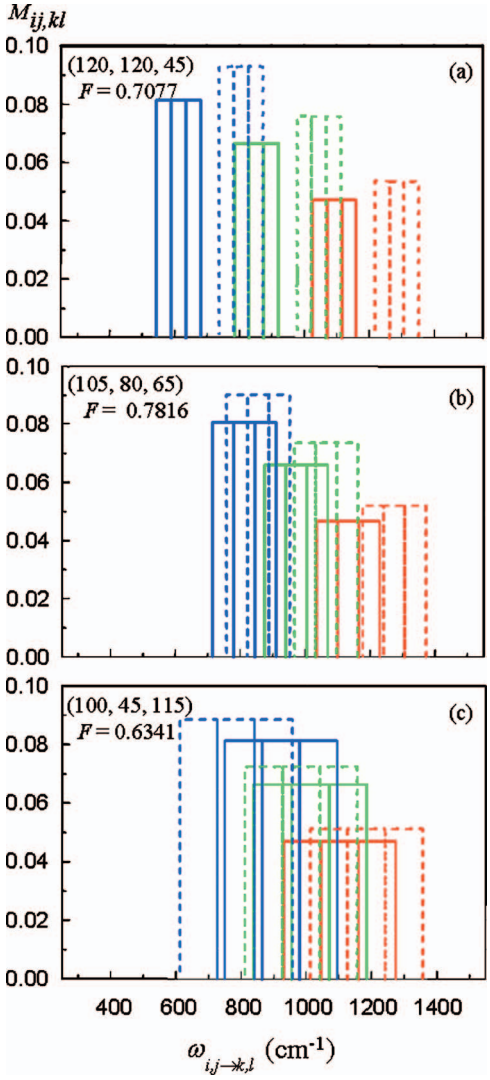


FIG. 8. (Color) Transition frequency diagrams for three typical points from the A/B plane. All twenty four frequencies are shown. Several resonances can be found in each case. Compared to these pictures, the frequency diagram of Fig. 3 is very clean.

effect is given in Fig. 6(c). Here one of the transitions in the target qubit, $|10\rangle \rightarrow |11\rangle$, is in resonance with the $|10\rangle \rightarrow |20\rangle$ transition, which basically connects it to a two-dimensional ladder of transitions into many upper states. Note that many of the resonant transitions correspond to the same initial or final state, which makes the leakage from the qubit very efficient and the selective control of state-to-state transitions very difficult. As a result, a dramatic reduction of the fidelity is observed.

Using Eq. (5) to express the frequencies of interfering transitions $|i,j\rangle \rightarrow |i,j+1\rangle$ and $|j+1,i-1\rangle \rightarrow |j+2,i-1\rangle$, we obtain for $j=0$ the relationship

$$\Delta_{12} = 4\Delta_1 - 2\Delta_2 + (\omega_2 - \omega_1). \tag{14}$$

Note that this formula links the values of all three anharmonicity parameters but also includes the difference between the values of harmonic frequencies $\omega_1$ and $\omega_2$. The plane in the $(\Delta_1,\Delta_2,\Delta_{12})$ space defined by Eq. (14) is not parallel to any axis and this is consistent with the results of optimization presented in Fig. 4(c). For $j=1$ the relationship is

$$\Delta_{12} = 6\Delta_1 - 4\Delta_2 + (\omega_2 - \omega_1). \tag{15}$$

This plane is very close to plane (14). According to our optimization data, plane (14) plays the main role while plane (15) plays only a secondary role. But basically, both these features are responsible for the appearance of the gap between parts A and B, the A/B plane.

The A/B plane is, perhaps, the most complicated and important feature of the data cube. It explains why the fidelity drops between the regions A and B. It also explains why a system in which all three anharmonicity parameters are large ($\sim 100$ cm$^{-1}$) does not represent a good choice for the realization of the vibrational two-qubit system. This is simply because in the data cube the A/B plane passes very close to this region of the $(\Delta_1,\Delta_2,\Delta_{12})$ space.

### E. Effect of frequencies

An important feature of the A/B plane is its dependence on the value of $(\omega_2-\omega_1)$, which represents the detuning between the harmonic frequencies of the target and the control qubits. In our case $\omega_1=1615$ cm$^{-1}$ and $\omega_2=1423$ cm$^{-1}$ and the value of detuning is negative, $-192$ cm$^{-1}$. Note that our choice of these frequencies was made rather arbitrarily and since we are studying a general model where all the parameters can be varied it makes sense to ask what would happen if we try different frequencies and change the value of detuning. From Eq. (14) it follows that making detuning more negative would move the A/B plane towards a larger value of $\Delta_1$ and a smaller value of $\Delta_2$. This means that the low fidelity A/B plane would move away from the A region but further into the B region. The size of the A region would significantly increase and the fidelity in a large part of it would improve. Since the A region is more attractive for the realization of the vibrational QC such a change would increase our chances of having a good control over the two-qubit system. Thus, it is advantageous to have a large negative value of detuning, which also means that $\omega_1 > \omega_2$ is the right choice for the two-qubit system. Note that an opposite change, i.e., making the value of detuning less negative or even positive, would move the A/B plane towards the A region and reduce the fidelity here. Roughly, at $(\omega_2-\omega_1)=-80$ cm$^{-1}$ the A/B plane would start adversely affecting the lower corner of the $A_1$ region, where the systems are characterized by intermediate values of $\Delta_2$. At $(\omega_2-\omega_1)\sim 0$ the A/B plane would move right into the middle of the high fidelity region and would probably destroy it completely.

## IV. CONCLUSION

In this paper we studied a two-qubit system encoded into two normal vibration modes of a molecule. We focused on understanding how the anharmonic properties of the molecule affect its controllability by the femtosecond shaped laser pulses. In order to represent the molecule we developed a general model which uses basic spectral characteristics ($\omega_1$, $\omega_2$, $\Delta_1$, $\Delta_2$, and $\Delta_{12}$) and enables us to easily vary these parameters in a wide range. We varied the values of three anharmonicity parameters independently in the range from 40 to 120 cm$^{-1}$ and, for each case, used the optimal control theory to derive the shaped pulse that could serve as quantum gate CNOT. We observed that the dependence of the fidelity of the quantum gate, used here as a measure of controllability of a system, is rather complicated and is governed by the presence (or lack) of interference between the transitions in the target qubit and the transitions into upper vibrational states, including the states of the control mode.

We identified three main regions in the $(\Delta_1,\Delta_2,\Delta_{12})$ parameter space where the fidelity of qubit transformation is particularly high. We also found that these regions are separated by three planar regions where the fidelity is very low. The origin of these low fidelity planes is now well understood and their location in the $(\Delta_1,\Delta_2,\Delta_{12})$ space is well defined in terms of very general analytic relationships (12)–(14) between the anharmonicity parameters and harmonic frequencies of the two-qubit system. When choosing a candidate molecule for the practical implementation of the vibrational QC one should try to avoid these regions. A simple advice is to stay at least 15 cm$^{-1}$ from each plane. Qualitatively, one can still use a picture of a three-dimensional high fidelity plateau but should have in mind that this plateau is crossed by several "canyons" where the fidelity drops dramatically.

The maximum fidelity we observed was very high ($F_{\max}=0.9997$) and occurred at the point $(\Delta_1,\Delta_2,\Delta_{12})=(55,120,65$ cm$^{-1})$ on the edge of our data cube. A very important finding is that this point is not a special or rare case, instead, it belongs to a rather large region in the $(\Delta_1,\Delta_2,\Delta_{12})$ space where the fidelity is persistently high, $F>0.999$. Choosing a molecule with such properties will guarantee a very high fidelity of the quantum gates using simple-shaped subpicosecond laser pulses, such as the pulse shown in Fig. 2(a).

Note that such a high fidelity requires relatively large values of several anharmonicity parameters simultaneously—a property which may be difficult to find in real molecules. Therefore, we tried to find a region in the data cube where the values of the three anharmonicity pa-

rameters are as small as possible but the fidelity of qubit transformations is still reasonably high. We located such a spot in the lower corner of the $A_1$ region. An example point from this region is $(\Delta_1,\Delta_2,\Delta_{12})=(40,70,40\ \mathrm{cm}^{-1})$ where the fidelity of 750 fs gate CNOT is on the order of 0.99. Note that these values of anharmonicity parameters are reasonably low. Still, the value of $\Delta_2$ must be about twice as large as the values of $\Delta_1$ and $\Delta_{12}$. Moreover, further analysis of the data cube indicates that this feature must have some continuation into the range of even smaller values of all three anharmonicity parameters. We did not study the range of $\Delta$'s below 40 $\mathrm{cm}^{-1}$ extensively in the paper but we carried out optimization at several points from that region and achieved the fidelity on the order of 0.99 at $(\Delta_1,\Delta_2,\Delta_{12})=(35,75,35\ \mathrm{cm}^{-1})$. We conclude that this region in the $(\Delta_1,\Delta_2,\Delta_{12})$ space is, perhaps, the most attractive for the first experimental work aimed at the proof of principle. Note that in order to keep the A/B plane away from this region the value of detuning of two harmonic frequencies must be large and negative, at least $(\omega_2-\omega_1)=-100\ \mathrm{cm}^{-1}$.

Apparently, the $MnBr(CO)_5$ case studied in Ref. 17 does not seem to be a very successful choice due to a relatively small frequency difference of the two vibration modes and relatively low anharmonicity parameters. According to the rms fit using the standard Dunham expansion of the data in Table I of Ref. 17, for $MnBr(CO)_5$ we obtained $\omega_1=2089\ \mathrm{cm}^{-1}$, $\omega_2=2097\ \mathrm{cm}^{-1}$, $\Delta_1=10.1\ \mathrm{cm}^{-1}$, $\Delta_2=11.4\ \mathrm{cm}^{-1}$, and $\Delta_{12}=-5.9\ \mathrm{cm}^{-1}$. We believe that for this reason the gate pulse duration had to be increased by an order of magnitude up to 9 ps in order to obtain accurate qubit transformations.[17]

When we were finalizing this work and preparing it for publication we found out that a very relevant paper had been published by Vivie-Riedel's group in the New Journal of Physics.[31] Their analysis allowed them to distinguish between the two fundamentally different mechanisms of qubit transformations and also provided new and important insight into the processes in the vibrational quantum computer. Furthermore, they showed that the requirement of a large anharmonicity (which we formulated for a one-qubit system) holds for the target qubit of the two-qubit system as well. Note that the authors of Ref. 31 adopted our idea of changing the anharmonicity of a model system but they did it in a different way, namely, by changing the shape of the potential energy surface along the two vibration modes, solving for two-dimensional eigenstates and energies in each case and then using those in the pulse optimization procedure. We believe that their approach is not only more complicated and computationally demanding but may finally be even less accurate compared to the straightforward method we use in this work. We directly model the vibrational spectrum and the dipole moment matrix elements of a molecule, which allows us to avoid the costly calculations of the vibrational wave functions and thus exclude errors always present in the theoretical treatment of molecular properties and of the character of the vibration modes. (For example, see the discussion in Sec. II of Ref. 17.) Our approach is clearly more flexible; it can be easily extended onto more-then-two-qubit system or applied to a real molecule if the minimal information about the vibration frequencies and anharmonicities is available from the experiment or the electronic structure calculations.

The second advantage of the work reported here is a systematic study of the effect of all three anharmonicity parameters ($\Delta_1$, $\Delta_2$, and $\Delta_{12}$) on the accuracy of gates achieved with the subpicosecond pulses. Note that Ref. 31 focused mainly on the effect of the anharmonicity of the target qubit, with somewhat less attention pointed to the effect of the intermode coupling, and only said little about the control qubit. Only a very limited number of sets of parameters (12) were considered in Ref. 31, which did not allow the authors of that work to see several important general effects. Our approach allowed us to study a much broader variety of anharmonicity parameters which resulted in a qualitatively different insight.

All the assumptions used in our model are justified by the fact that the vibrational excitation is very low and the vibrational wave function of the molecule is localized near its equilibrium point. As a result, we do not need to calculate the multidimensional potential energy surface and dipole moment functions, instead, the molecular structure optimization followed by single point calculations of harmonic frequencies, anharmonicities, and dipole moments should be enough. It may be argued that anharmonicities obtained by a single point electronic structure calculation may not be very accurate, especially if the potential energy surface is complicated. This does not represent any problem for the work reported here because the values of anharmonicities were anyway varied in a broad range. In the case when the coherent control of a given molecule should be modeled theoretically as accurately as possible (in order to better explore the feasibility of experimental implementation of a chosen candidate, for example) our approach can still be employed using experimentally measured frequencies, anharmonicities, and dipole moments as inputs. In this way the theoretical errors in the description of molecular properties and environmental effects (such as a solvent effect) can be eliminated. We believe that the accuracy of such a *hybrid* approach may exceed the accuracy of the methods where all the molecular properties are determined *ab initio*.

## ACKNOWLEDGMENTS

This research was partially supported by NSF Grant No. PHY-045953. It also used resources of the National Energy Research Scientific Computing (NERSC) Center, supported by the Office of Science of the U.S. Department of Energy under Contract No. DE-AC03-76SF00098.

[1] C. M. Tesch, L. Kurtz, and R. de Vivie-Riedle, Chem. Phys. Lett. **343**, 633 (2001).
[2] W. Zhu, J. Botina, and H. Rabitz, J. Chem. Phys. **108**, 1953 (1998).
[3] A. Assion, T. Baumert, M. Bergt, T. Brixner, B. Kiefer, V. Seyfried, M. Strehle, and G. Gerber, Science **282**, 919 (1998).
[4] R. A. Bartels, S. Backus, E. Zeek, L. Misoguti, G. Vdovin, I. P. Christov, M. M. Murnane, and H. C. Kapteyn, Nature (London) **406**, 164 (2000).
[5] F. G. Omenetto, A. J. Taylor, M. D. Moores, and D. H. Reitze, Opt. Lett. **26**, 938 (2001).
[6] M. Jacoby, C&EN **84**, 7 (2006).
[7] L. Windhorn, T. Witte, J. S. Yeston, D. Proch, M. Motzkus, K. L. Kompa, and W. Fuß, Chem. Phys. Lett. **357**, 85 (2002).
[8] D. Zeidler, S. Frey, W. Wohlleben, M. Motzkus, F. Busch, T. Chen, W.

Kiefer, and A. Materny, J. Chem. Phys. **116**, 5231 (2002).
[9] T. Witte, T. Hrnung, L. Windhorn, D. Proch, R. de Vivie-Riedle, M. Motzkus, and K. L. Kompa, J. Chem. Phys. **118**, 2021 (2003).
[10] C. M. Tesch and R. de Vivie-Riedle, Phys. Rev. Lett. **89**, 157901 (2002).
[11] U. Troppmann, C. M. Tesch, and R. de Vivie-Riedle, Chem. Phys. Lett. **378**, 273 (2003).
[12] U. Troppmann and R. de Vivie-Riedle, J. Chem. Phys. **122**, 154105 (2005).
[13] C. M. Tesch, K.-L. Kompa, and R. de. Vivie-Riedle, Chem. Phys. **267**, 173 (2001).
[14] D. Babikov, J. Chem. Phys. **121**, 7577 (2004).
[15] T. Cheng and A. Brown, J. Chem. Phys. **124**, 034111 (2006).
[16] Y. Ohtsuki, Chem. Phys. Lett. **404**, 126 (2005).
[17] B. M. R. Korff, U. Troppmann, K. L. Kompa, and R. de. Vivie-Riedle, J. Chem. Phys. **123**, 244509 (2005).
[18] S. Suzuki, K. Mishima and K. Yamashita, Chem. Phys. Lett. **410**, 358 (2005).
[19] C. M. Tesch and R. de Vivie-Riedle, J. Chem. Phys. **121**, 12158 (2004).
[20] M. Zhao and D. Babikov, J. Chem. Phys. **125**, 024105 (2006).
[21] U. Troppmann, C. Gollub, and R. de Vivie-Riedle, New J. Phys. **8**, 100 (2006).
[22] T. Cheng and A. Brown, J. Chem. Phys. **124**, 144109 (2006).
[23] E. L. Sibert III and M. Gruebele, J. Chem. Phys. **124**, 024317 (2006).
[24] D. Weidinger and M. Gruebele, Phys. Rev. A (submitted).
[25] J. P. Palao and R. Kosloff, Phys. Rev. Lett. **89**, 188301 (2002).
[26] J. P. Palao and R. Kosloff, Phys. Rev. A **68**, 062308 (2003).
[27] R. Zadoyan, D. Kohen, D. A. Lidar, and V. A. Apkarian, Chem. Phys. **266**, 323 (2001).
[28] Z. Bihary, D. R. Clenn, D. A. Lidar, and V. A. Apkarian, Chem. Phys. Lett. **360**, 459 (2002).
[29] D. R. Clenn, D. A. Lidar, and V. A. Apkarian, Mol. Phys. **104**, 1249 (2006).
[30] J. Vala, Z. Amitay, B. Zhang, S. R. Leone, and R. Kosloff, Phys. Rev. A **66**, 062316 (2002).
[31] C. Gollub, U. Troppmann, and R. De Vivie-Riedle, New J. Phys. **8**, 48 (2006).
[32] C. Tao, M. Deselnicu, C. Mukarakate, and S. A. Reid, J. Chem. Phys. **125**, 094305 (2006).
[33] D. Babikov, V. A. Mozhayskiy, and A. I. Krylov, J. Chem. Phys. **125**, 084306 (2006).
[34] D. James, S. McGrane, D. Babikov, G. Rodriguez, A. Efimov, and A. Taylor (unpublished).
[35] M. J. Frisch, G. W. Trucks, and H. B. Schlegel *et al.*, GAUSSIAN03, Revision A.1 (Gaussian, Inc., Pittsburgh, PA, 2003).
[36] E. B. Wilson Jr., J. C. Decius, and P. C. Cross, *Molecular Vibrations* (Dover, New York, 1955), p. 38.
[37] W. Demtroder, *Molecular Physics* (Wiley-VCH, Weinheim, 2005), p. 279.
[38] K. Sundermann and R. de Vivie-Riedle, J. Chem. Phys. **110**, 1896 (1999).
[39] K. Sundermann, H. Rabitz, and R. de Vivie-Riedle, Phys. Rev. A **62**, 013409 (2000).